INFLUENCE OF FLUID RHEOLOGY ON BLOOD FLOW HAEMODYNAMICS IN PATIENT-SPECIFIC ARTERIAL NETWORKS OF VARIED COMPLEXITY – IN-SILICO STUDIES

Zbigniew TYFA*, Piotr REOROWICZ*, Damian OBIDOWSKI*, Krzysztof JÓŹWIK*

*Faculty of Mechanical Engineering, Lodz University of Technology,
Żeromskiego 116 St., 90-924 Łódź, Poland

zbigniew.tyfa@p.lodz.pl, piotr.reorowicz@p.lodz.pl, damian.obidowski@p.lodz.pl, krzysztof.jozwik@p.lodz.pl

received 30 March 2023, revised 5 June 2023, accepted 28 June 2023

Abstract: Results obtained with computational fluid dynamics (CFD) rely on assumptions made during a pre-processing stage, including a mathematical description of a fluid rheology. Up to this date there is no clear answer to several aspects, mainly related to the question of whether and under what conditions blood can be simplified to a Newtonian fluid during CFD analyses. Different research groups present contradictory results, leaving the question unanswered. Therefore, the objective of this research was to perform steady-state and pulsatile blood flow simulations using eight different rheological models in geometries of varying complexity. A qualitative comparison of shear- and viscosity-related parameters showed no meaningful discrepancies, but a quantitative analysis revealed significant differences, especially in the magnitudes of wall shear stress (WSS) and its gradient (WSSG). We suggest that for the large arteries blood should be modelled as a non-Newtonian fluid, whereas for the cerebral vasculature the assumption of blood as a simple Newtonian fluid can be treated as a valid simplification.

Key words: blood rheology; CFD; non-Newtonian blood flows; arterial systems

1. INTRODUCTION

Computational fluid dynamics (CFD) tools can be considered as numerical simulations that help predict and analyse the physical behaviour and complex phenomena occurring in fluid flows by solving equations of fluid mechanics, i.e. energy, mass and momentum conservation. As far as simulations of blood flow are concerned, CFD can provide an insight into the flow structures of a given patient without exposing him or her to any health risks. Furthermore, in-silico analyses can provide valuable preoperative information to help medical professionals plan and perform surgery. However, it should not be left unmentioned that the results of any numerical simulation depend heavily on initial assumptions made during a pre-processing stage. Apart from the complexity of the arterial system or the inflow and outflow boundary conditions, one such assumption is a mathematical description of the rheology of the fluid.

In fluid mechanics, there are three fundamental parameters of any fluid, namely heat conductivity, density and viscosity. Since the main heat transfer occurs in capillaries, not arteries, in the vast majority of CFD studies blood flow is modelled as isothermal and adiabatic – there is no heat transfer, and thus the first parameter (heat conductivity) can be neglected. In terms of density, blood is usually considered to be an incompressible fluid (although it carries O2 and CO2). Its density is in the range of 1,030–1,070 kg/m3 [1] .

The last parameter, viscosity, can be described as the resistance of a fluid to flow. Resistive viscous forces arise due to mutual attractive forces between fluid particles. In terms of bioflows, the importance of viscosity is related to the fact that it partially controls the blood flow through arteries and veins. For instance, a higher haematocrit value (ratio of red blood cells in blood) results in a viscosity increase and, consequently, higher resistances for the flow [2]. In general, blood is a complex fluid that exhibits non-Newtonian shear-thinning behaviour. This means that its viscosity varies when subjected to external stress – the higher the shear rate, the lower the viscosity. This can be observed when the blood velocity is high or when the vessel cross-section is relatively small. Shear-thinning phenomenon occurs at higher shear rates because erythrocytes and other blood cells begin to deform under applied stress. Otherwise, they form aggregates that increase the attractive forces between them, leading to a higher viscosity and, consequently, higher flow resistance [2].

The non-Newtonian properties of blood are significant at lower values of shear rate – it is claimed that after exceeding the 100 s–1 threshold, blood can be treated as a simple Newtonian fluid of constant viscosity [3,4]. Similarly, as with any experimental study of living tissue, varied research groups have obtained different results regarding the shear-thinning behaviour of blood. This is due to the fact that blood is a patient-specific fluid (its parameters depend on numerous factors such as sex, age, diet, general hydration, medications taken, etc.), and thus all its physical properties vary widely among the human population. Therefore, dozens of different mathematical formulas describing blood have appeared in the literature. Tab. 1 and Fig. 1 present the most common rheological models that are widely used for in-silico studies of blood flow.

As stated before, the non-Newtonian properties of blood are significant at lower values of shear rates, i.e. <100 s–1 [3,4]. It is claimed that shear rates are high in large arteries or vessels characterised by high blood flow and relatively small size. Therefore, it

sciendo
DOI 10.2478/ama-2024-0002

is hypothesised that the Newtonian assumption is valid for the majority of human arteries [2]. However, the shear rate can vary throughout the entire cardiac cycle from 0 s–1 to 1,000 s–1, and thus the assumption of a non-Newtonian shear-thinning fluid seems to be mandatory to obtain the most realistic numerical results [9]. Therefore, many scientists have analysed the influence of blood rheology on CFD data. Unfortunately, there is no clear answer as to whether blood can be simplified to a Newtonian fluid – each research group has presented slightly different results and drawn contradictory conclusions.

Tab. 1. The most common rheological models of blood used in CFD

Blood model	Mathematical formula	
Newtonian (NEWT)	$\eta = 0.00345\ \text{Pa}\cdot\text{s}$ $\eta = 0.0035\ \text{Pa}\cdot\text{s}$	(1)
Power Law (PL)	$\eta = k\cdot(\dot{\gamma})^{n-1}$ where: k = 0.017 kg · m^{-1} · s$^{-1.292}$; n = 0.708	(2)
Quemada (QUE)	$\eta = \eta_p\cdot(1-\frac{K\cdot HTC}{2})^{-2}$ $K = \frac{k_0 + k_\infty\cdot(\dot{\gamma}/\dot{\gamma}_c)^{0.5}}{1+(\dot{\gamma}/\dot{\gamma}_c)^{0.5}}$ where: η_p = 0.00127 Pa·s; k_0 = 4.0; k_∞ = 1.5; $\dot{\gamma}_c$ = 5.0 s^{-1}	(3)
Modified PL (MPL) (1,5–8)	$\begin{cases}\eta = 0.55471\ \text{Pa}\cdot\text{s} & \text{for } \dot{\gamma}\le 0.001\\ \eta = \eta_0\cdot(\dot{\gamma})^{n-1} & \text{for } 0.001 \le \dot{\gamma} < 327\\ \eta = 0.00345\ \text{Pa}\cdot\text{s} & \text{for } \dot{\gamma}\ge 327\end{cases}$ where: η_0 = 0.035 kg · m^{-1} · s$^{-1.4}$; n = 0.6	(4)
Carreau (CAR)	$\eta = \eta_\infty + (\eta_0-\eta_\infty)\cdot(1+(\lambda\cdot\dot{\gamma})^2)^{\frac{n-1}{2}}$ where: η_∞ = 0.0035 Pa·s; η_0 = 0.056 Pa·s; λ = 3.313005 s; n = 0.3568;	(5)
Casson (CAS)	$\eta = (\sqrt{\eta_c} + \sqrt{\frac{\tau_c}{\dot{\gamma}}})^2$ where: η_c = 0.00414 kg · m^{-1} · s^{-1}; τ_c = 0.0038 kg · m^{-1} · s^{-2}	(6)
Cross (CRO)	$\eta = \eta_\infty + \frac{\eta_0-\eta_\infty}{1+(\lambda\cdot\dot{\gamma})^a}$ where: η_∞ = 0.0035 Pa·s; η_0 = 0.0364 Pa·s; λ = 0.38 s; a = 1.45	(7)
K-L (KL)	$\eta = \frac{1}{\dot{\gamma}}\cdot(\tau_c + \eta_c\cdot(a_2\cdot\sqrt{\dot{\gamma}} + a_1\cdot\dot{\gamma}))$ where: τ_c = 0.005 Pa; η_c = 0.0035 Pa; a_1 = 1.0 s; a_2 = 1.19523 s$^{0.5}$	(8)

One of the first numerical studies of rheology was proposed by Gijsen et al. [10]. Their research showed that the non-Newtonian fluid (Carreau–Yasuda model) has a considerable effect on the flow velocity in the carotid arteries when compared to the results for a simple Newtonian fluid. Thus, this indicates that the rheology of blood plays a critical role in the ability of the numerical solver to properly approximate the flow distribution. Shinde et al. [11] stated that if shear stress is meant to be considered as a predictor of atherosclerosis development, a non-Newtonian fluid should be assumed. In contrast, Boyd and Buick [12], who also analysed the carotid artery as well, concluded that the non-Newtonian properties of blood can be neglected due to small relative differences between rheological models. Mendieta et al. [13] suggested that Newtonian fluid is a reasonable assumption when analysing averaged shear stress, oscillatory shear index and general flow distribution. The next CFD study using the carotid artery was prepared by Razavi et al. [14], who analysed the influence of Newtonian and six non-Newtonian models on flow haemodynamics. After performing a series of transient simulations, they found that even at high velocities (and consequently high shear rates), considerable differences were detectable for Power Law and Walburn–Schneck models. Razavi et al. [14] concluded that the Power Law overestimated wall shear stress (WSS) values at both low and high shear rates, while the Generalized Power Law and modified Casson models appeared to underestimate the non-Newtonian behaviour. According to this scientific group, the Carreau and Carreau–Yasuda models are the most appropriate rheological approximations of the human blood flow in the carotid artery. Furthermore, their research has shown that the assumption of pulsatile flow is mandatory for the study of recirculation phenomena, which can lead to drastic changes in shear rates and, consequently, in viscosity – such an analysis cannot be performed for the steady-state simulations [14].

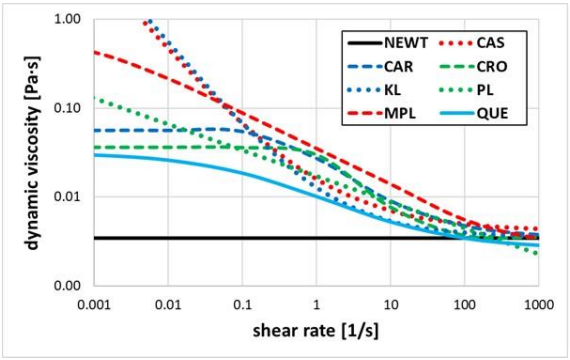

Fig. 1. Dynamic viscosity dependence on shear rate (logarithmic plots) – the most common rheological blood models

In 2004 and 2006 Johnston et al. [4,15] carried out steady-state and pulsatile blood flow simulations in patient-specific coronary arteries. The results of these studies showed that the shear stress distribution at the arterial walls was consistent for all rheological models (Newtonian, Power Law, Carreau, Casson, Walburn–Schneck and Generalized Power Law), although magnitudes varied. For the steady-state simulations, Johnston et al. observed that the WSS differences between the rheological models became less distinct as the inlet velocity increased (associated with a concomitant increase in shear rate).

To quantitatively compare the viscosity differences between each non-Newtonian and Newtonian model, this research group introduced two parameters: local and global non-Newtonian importance factors. These parameters are described more thoroughly in the further part of this paper. The results indicated that for the flows characterised by medium to high shear rates, the Newtonian model is a valid approximation. By comparing steady-state and transient results, Johnston et al. concluded that the Newtonian blood model is a reliable assumption for approximately 70% of the cardiac cycle. During the remaining 30%, the flow was characterised by relatively lower velocity, which increased the viscosity and consequently WSS values. Therefore, they suggested that the Newtonian model may be a reasonable and sufficient approximation for transient simulations [15]. However, they emphasised that the non-Newtonian model of blood should be used for in-depth

studies focussing on local haemodynamics, such as vortex formation.

To evaluate the impact of the rheological model on haemodynamics within the largest vessel of the human organism, Karimi et al. [16] generated a patient-specific model of the aorta consisting of ascending aorta, aortic arch and initial region of descending aorta. They performed transient simulations and investigated the following blood models: Newtonian, Casson, K-L, Modified Casson, Carreau, Carreau–Yasuda, Cross, Power Law, Modified Power Law and Generalized Power Law. It was ascertained that the Cross model generates significantly different WSS and velocity distributions at diastole (when shear rates are low) when compared to other non-Newtonian models. Moreover, this thorough and extensive research proved that blood rheology affects the flow solution, while the Newtonian assumption tends to underestimate WSS values [16].

Caballero and Lain [2] investigated the influence of rheology in a slightly more complex geometry of the aorta, since it extended up to the abdominal region. They performed steady-state and transient in-silico analyses in which the blood was described by the following rheological models: Newtonian, Carreau, Power Law and Herschel–Buckley. Similar to the previous studies, they found that the WSS distribution was consistent across all rheological cases, but WSS magnitudes varied, especially at lower inlet velocities. For medium to high shear rates, little differences were observed. Their results indicated that Carreau and Herschel–Buckley models tended to overestimate WSS at high velocities, while the Newtonian model underestimated WSS at low flow rates. Moreover, when they compared the cycle-averaged results for all rheological models, there were hardly any differences in WSS and the global non-Newtonian importance factor, indicating that the non-Newtonian model assumption is not of great significance for pulsatile flow. Therefore, Caballero and Laín [2] concluded that the Newtonian model is a suitable assumption for the transient analysis.

Shortly thereafter, Doost et al. [3] analysed haemodynamics within patient-specific geometry of the left ventricle. During transient simulations, blood was modelled as Newtonian and non-Newtonian fluid (described by Carreau, Casson, Generalized Power Law, K-L and Cross equations). It has been shown that the choice of the specific rheological model has a considerable influence on the obtained results. For instance, each mathematical description of blood resulted in different numbers and sizes of small vortices. The results of the K-L and Cross models produced lower WSS values than pure Newtonian fluid, whereas the WSS values for the other rheological models were significantly higher [3].

Considering all the aforementioned information (derived from the available literature), it can be concluded that there is no clear answer whether blood can be simplified to a Newtonian fluid for in-silico investigations or whether it has to be considered as a specific non-Newtonian fluid. Each research group presents different results and varied conclusions, and thus the answer remains ambiguous. Therefore, the main objective of this research was to evaluate the influence of the chosen blood model on the numerical data by performing steady-state and pulsatile blood flow simulations relying on eight different blood models in patient-specific geometries of varying complexity. This could help to answer three open hypotheses:

- blood can be simplified to a Newtonian fluid in large arteries and small vessels with high blood flow;
- blood can be simplified to a Newtonian fluid for cycle-averaged and steady-state investigations;
- regardless of vessel size, when blood flow is characterised by low intensity, the effect of viscosity variation is so pronounced that the use of shear rate-dependent models is recommended.

2. MATERIALS AND METHODS

To accomplish all of the objectives of the following research, numerous separate steps had to be taken. Firstly, one had to prepare several patient-specific geometries of varying complexity. Then, volumetric meshes of sufficient quality had to be generated. Finally, the authors performed steady-state and pulsatile blood flow simulations, considering blood washout analysis. All these steps are briefly described in the further part of this paper.

2.1. Patient-specific geometries

As described earlier, blood viscosity depends on numerous factors, including the topology of the flow channels, and thus it was decided to carry out an analysis of blood rheology in geometries of varying complexity: a simple bifurcation of the common carotid artery (CCA), the entire aorta with major branches and a complex system of intracranial arteries. All patient-specific models (see Fig. 2) were reconstructed from biomedical imaging that was subjected to image segmentation procedures. Model retrieval methods were performed in a custom software called Anatomical Model Reconstructor (AMR) developed at the Institute of Turbomachinery (Lodz University of Technology, Poland).

The first step was to import Digital Imaging and Communications in Medicine (DICOM) images obtained by angiography computed tomography (angio-CT) into the AMR software. Then, each voxel in the dataset was divided into eight sub-voxels to improve automatic segmentation procedures. To visualise arteries filled with a contrast agent (to distinguish them from surrounding tissues), a specific preset of the windowing operation was used. Then, the region growing method was used to perform image segmentation for the entire image set. Unfortunately, each 3D mask required further manual processing. The main shortcomings were related to the separation of bone structures from the arterial lumen and the addition of smaller branches of intracranial vessels that were omitted during the automatic image segmentation. Once a 3D binary mask was completed and stored for all the regions of interest (lumens of the selected blood vessels), a 3D surface geometry of the given arterial network was extracted from it. The voxelised model (with staircase-like topology) was smoothed with expert smoothing parameters to obtain an anatomically correct model while preserving the overall topology. Then, each arterial branch was clipped in its proximal or distal part to obtain perpendicular cross-sections for the outlet and inlet surfaces. The next step was to cover each open channel with a planar surface using an automated capping method. This means that each opening or hole detected in the wall of the model was automatically filled with a simple planar surface that was treated as a separate 3D object. Finally, each relevant 3D surface model, i.e. the artery wall and all capping boundaries, was saved to a selected folder as a separate file stored in stereolithography (STL) format. Fig. 2 depicts a comparison of all three patient-specific models, generated in the custom-developed AMR software, that were used during this research.

DOI 10.2478/ama-2024-0002

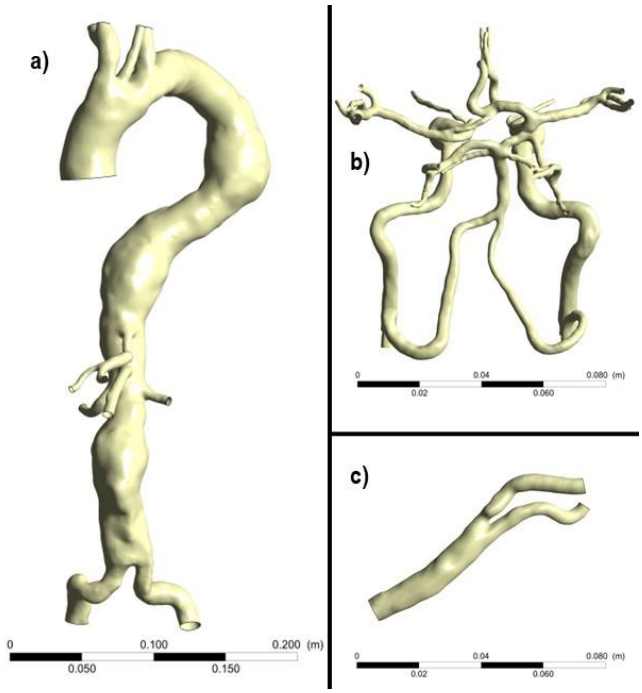

Fig. 2. Patient-specific models used during in-silico investigations: (a) entire aorta with major branches; (b) complex intracranial arterial system; (c) carotid artery bifurcation

2.2. Numerical domain: volumetric meshes

High-quality volumetric meshes were generated in the ANSYS ICEM (Ansys Inc. Canonsburg, USA) package, based on prepared STL objects. They consisted of unstructured tetrahedral elements in the free-flow regime as well as prismatic elements embedded in an inflation layer. The inflation layer was composed of 16 sublayers – such a number was chosen after thorough sensitivity tests performed for each geometry type. Specific macro files were used for the mesh generation – such scripts were automatically prepared in the AMR software. Another aspect, also covered by a prepared script, focussed on the mesh metrics – each Delaunay mesh was subjected to additional smoothing and refinement to ensure that the resulting mesh was of high quality. This process was repeated thrice for tetrahedral elements and twice additionally for tetrahedral and prismatic elements. With each successive iteration, the ICEM mesh quality measure was increased.

Before focussing on target numerical simulations, it was necessary to ensure that a discretisation error due to the mesh density was negligible. Therefore, specific mesh independence tests (MITs), both asymptotic and parametric, were performed beforehand [17]. It was decided that the mesh for the carotid artery should comprise approximately two million elements, while the mesh for the intracranial arterial network should be composed of approximately six million elements. For the whole aorta, the coarsest mesh was chosen for further numerical analyses (consisting of about eight million elements).

2.3. Numerical domain: simulation settings

In all simulations, i.e. steady-state and transient, the flow was assumed to be adiabatic and isothermal, while blood was treated as an incompressible fluid with constant density (1,045 kg/m3) and varying viscosity, as defined by eight specific models, which are presented in Tab. 1. The flow simulations were performed using the pressure-based ANSYS CFX (Ansys Inc. Canonsburg, USA) solver. The Reynolds-averaged Navier–Stokes (RANS) equations were calculated with the k-ω Shear Stress Transport (SST) turbulence model. Each steady-state simulation was considered complete when it either reached the convergence criteria (10–6) or exceeded 500 iterations. The steady-state boundary conditions are listed in Tab. 2, while the transient boundary conditions for the inlet cross-sections are shown in Fig. 3. A Prandtl velocity profile was set at the inlet cross-section in the aorta case study, whereas parabolic profiles were used for all the others. Static gauge pressure was set for each opening cross-section even in transient analyses, where the values were the same as in steady-state case studies. The reason for this simplification is the fact that the walls of the numerical domain were rigid, and thus the flow distribution depended only on the pressure gradient between the outlet surfaces.

Tab. 2. Steady-state boundary conditions used for the CFD analyses

<table>
<tr><th>Case</th><th colspan="4">Inlet cross-section max. velocity [m/s]</th><th colspan="2">Opening cross-sections pressure [kPa]</th></tr>
<tr><td rowspan="10">Entire aorta with major branches</td><td colspan="4" rowspan="10">0.12</td><td>Right SA</td><td>13.00</td></tr>
<tr><td>Right CCA</td><td>13.00</td></tr>
<tr><td>Left CCA</td><td>12.90</td></tr>
<tr><td>Left SA</td><td>13.015</td></tr>
<tr><td>HA</td><td>13.00</td></tr>
<tr><td>GA</td><td>13.00</td></tr>
<tr><td>SMA</td><td>13.00</td></tr>
<tr><td>Left RA</td><td>12.95</td></tr>
<tr><td>Right RA</td><td>12.95</td></tr>
<tr><td>Left CIA</td><td>13.01</td></tr>
<tr><td rowspan="2">CCA</td><td colspan="4" rowspan="2">0.85</td><td>Right CIA</td><td>13.02</td></tr>
<tr><td>ICA</td><td>14.00</td></tr>
<tr><td rowspan="2">Cerebral arteries</td><td>LICA</td><td>LVA</td><td>RICA</td><td>RVA</td><td colspan="2">All cerebral arteries</td></tr>
<tr><td>0.365</td><td>0.275</td><td>0.370</td><td>0.155</td><td colspan="2">11.00</td></tr>
<tr><td colspan="7">CCA, common carotid artery; CIA, common iliac artery; GA, gastric artery; HA, hepatic artery; LICA, left internal carotid artery; LVA, left vertebral artery; RA, renal artery; RICA, right internal carotid artery; RVA, right vertebral artery; SA, subclavian artery; SMA, superior mesenteric artery.</td></tr>
</table>

In addition, the blood washout phenomenon has been analysed in transient simulations, as it allows the detection of regions prone to stagnation and clotting since thrombus is expected to occur in regions of low velocity, low shear stress and non-washed-out areas [18,19]. In these studies, the washout analysis is based on the principle that “old blood” occupies an entire volume of the fluid domain at the beginning of the simulation. Then, “new blood” begins to flow inside the numerical domain, pushing “old blood” out of the domain according to the specification of the inlet boundary condition. No mixing of the two separate fluids (within a

single mesh element) was assumed. Both fluids were characterised by the same rheological properties.

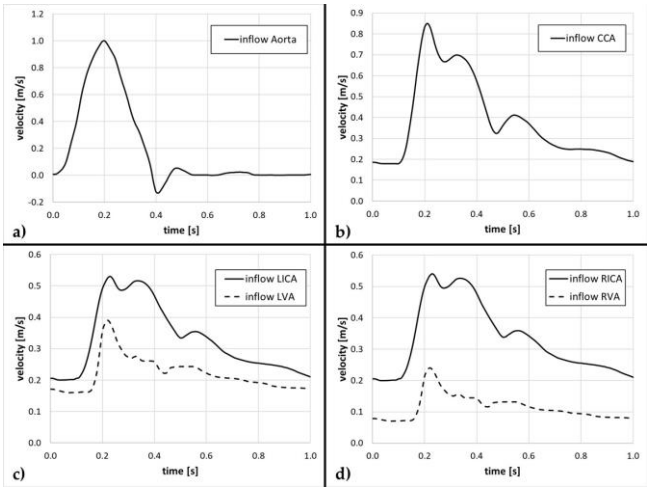

Fig. 3. Transient boundary conditions set on the inlet cross-sections in each analysed case study: (a) entire aorta; (b) carotid artery bifurcation; (c)–(d) intracranial arteries

The plots depicted in Fig. 3 are limited to just a single cardiac cycle for a higher clarity, but multiple cycles were simulated in the CFD analyses: 7 for the CCA bifurcation, 10 for the aorta and 5 for the cerebral vasculature. We wanted to minimise the influence of the initial conditions on the final results and to analyse a sufficient number of cardiac cycles required for a reliable blood washout analysis. Tab. 3 presents some parameters used for further comparison of the results.

Tab. 3. Chosen parameters used during the results' analysis

Parameter	Mathematical formula	
Time-averaged WSS (TAWSS) Shear stress averaged for one full cardiac cycle.	$\mathrm{TAWSS} = \frac{1}{T}\int_0^T \lvert\vec{\tau}_w\rvert dt$	(9)
WSS spatial gradient (WSSG) Determines regions of spatial changes in shear stress magnitude. High WSSG might indicate region prone to formation of atheromatous plaque or aneurysm growth.	$\mathrm{WSSG} = \sqrt{(\frac{\partial\vec{\tau}_{w,m}}{\partial m})^2 + (\frac{\partial\vec{\tau}_{w,n}}{\partial n})^2}$	(10)
Time-averaged WSSG (TAWSSG) WSSG averaged for full cardiac cycle.	$\mathrm{TAWSSG} = \frac{1}{T}\int_0^T WSSG dt$	(11)
Oscillatory shear index (OSI) Gives insight about the direction changes of shear forces throughout the cardiac cycle. High local OSI and low WSS show regions susceptible to plaque aggregation and instances of blood stagnation.	$\mathrm{OSI} = 0.5 \cdot (1 - \frac{\lvert\int_0^T \vec{\tau}_w dt\rvert}{\int_0^T \lvert\vec{\tau}_w\rvert dt})$	(12)
Local and global non-Newtonian importance factors (I_L and I_G) Describe local/global differences between dynamic viscosity produced by Newtonian and non-Newtonian fluids.	$\mathrm{I_L} = \frac{\eta}{\eta_\infty}$	(13)
	$\bar{\mathrm{I}}_\mathrm{G} = \frac{1}{N}\frac{[\sum_N(\eta-\eta_\infty)^2]^{1/2}}{\eta_\infty}$	(14)

3. RESULTS

To evaluate the influence of the rheological blood model on the numerical solution, numerous simulations were performed on a chosen geometry, i.e. CCA bifurcation, intracranial arterial network and entire aorta. Since eight different blood models were investigated for each selected reconstruction, a total of 48 simulations were performed (24 steady-state and 24 transient ones). To present the results clearly, each geometry is discussed separately. Besides an analysis of the most common flow parameters, i.e. velocity, wall shear stress (WSS) and flow distribution, several other haemodynamic indicators were estimated as well. To calculate them for steady-state and transient simulations, specific algorithms written in a high-level programming language (Python) were prepared. Thus, one could analyse TAWSS, OSI, WSSG, TAWSSG, IL and IG, which are described in Tab. 3.

However, before proceeding to the analysis of the rheology influence on the numerical data, it was decided to perform an initial validation of the results obtained. For this reason, the authors compared the basic haemodynamic parameters (estimated for Newtonian case studies) with the clinical and statistical research.

3.1. Results validation

Tabs. 4 and 5 provide information on the maximum velocity and Reynolds numbers recorded during peak systole for the CCA bifurcation and the entire aorta case studies. Moreover, Tab. 5 outlines data related to the relative blood distribution through three control surfaces: the common carotid artery and two renal arteries.

Tab. 4. Initial validation of the numerical data for the CCA bifurcation case study at systole peak – control plane located at CCA segment

Max. velocity [m/s]		Reynolds number [-]	
CFD data	**Reference**	**CFD data**	**Reference**
0.87	0.84* 0.89** 0.75*** 0.90**** 0.85*****	606	460 [5] 500 [20] 968 [21]
*Averaged value for female control group [22] **Averaged value for male control group [22] ***Value measured during resting conditions [23] ****Value measured during exercise [23] *****Value coming from ultrasonography examination [24]			

As can be seen, all the obtained results are in good agreement with the literature data – there are hardly any significant

discrepancies. It is worth mentioning that estimated Reynolds numbers (representing physiological in-vivo cases) seem to be low enough to treat the flow as laminar. This suggests that RANS closed with the k-ω SST turbulence model is not recommended for the assumed flows. However, it has to be stated that we simulated pulsatile blood flow in geometries with complex topology (consisting of numerous junctions and high curvature), which can affect the flow directioning. Thus, there was a high probability of occurrence of specific flow phenomena, such as flow separation and formation of recirculation zones. Therefore, treating the flow as a purely laminar one (which is suitable for fully developed flows that do not occur in the human circulatory system) might be an oversimplification. Moreover, as presented in Tabs. 4 and 5, the obtained results are consistent with the literature data, which proves that the numerical domain assumptions were correct.

Tab. 5. Initial validation of the numerical data for the entire aorta case study and several chosen control surfaces

	Relative blood distribution with respect to the inflow		Reynolds number at systole peak [-]	
Location	**CFD data**	**Reference**	**CFD data**	**Reference**
CCA	10.6%	8.5% (25)	844	460 [5] 500 [20] 968 [21]
Left RA	7.72%	8.6% (25)	673	400–1,100 [26]
Right RA	7.25%	8.6% (25)	800	
CCA, common carotid artery; RA, renal artery.				

Regarding the cerebral vasculature, it was decided to analyse the symmetry of blood supply between both hemispheres of the brain and its relation to the cardiac output (Tab. 6). Since the spatial geometry was limited to intracranial arteries (it did not start at the aorta), it was decided to assume 70 cm3 as a reference for physiological cardiac output [27]. Moreover, the authors presented volume flow rates at three main control surfaces located at the left and right middle cerebral arteries as well as at the basilar artery (Tab. 7).

Tab. 6. Initial validation of the numerical data for the cerebral vasculature case study – part one

Location	**Blood volume delivered in one full cardiac cycle [cm^3]**	**Relative ratio**	**Referential ratio**
Left hemisphere	4.869	50.1% of the inflow	50%–50% (symmetry)
Right hemisphere	4.851	49.9% of the inflow	
Full vasculature	9.720	13.89% of the physiological cardiac output (70 cm^3)	15% of the cardiac output [28,29] 14.4% of the cardiac output [25] 13%–15% of the cardiac output [30]

Tab. 7. Initial validation of the numerical data for the cerebral vasculature case study – part two

Location	**Volume flow rate [cm^3/min]**	
	CFD data	**Reference**
Basilar artery	178	182 ± 56 [31] 138 ± 41 [32] 145 ± 41 [33]
Left middle cerebral artery	160	159 ± 28 [32] 146 ± 31 [33]
Right middle cerebral artery	138	146 ± 28 [32] 146 ± 31 [33]

As shown in Tab. 6, the CFD-estimated flow distribution represents a physiologically correct blood supply. Not only is the flow distributed symmetrically between both hemispheres of the brain (50.1% for the left hemisphere and 49.9% for the right one), but also the total volume of blood supply, i.e. 9.72 cm3, represents approximately 14% of the physiological cardiac output. Thus, we confirmed that our results correlate well with clinical observations [25,28–30].

Regarding the volume flow rates at three control planes (see Tab. 7), the obtained results are again in a correct physiological range. For example, the reference volume flow rate through the left middle cerebral artery is reported to be 159 ± 28 cm3/min [32], whereas the result obtained from our simulations is equal to 160 cm3/min.

Considering all the presented information, it can be concluded that the performed in-silico analyses of blood flow in each arterial configuration (i.e. CCA bifurcation, entire aorta and cerebral vasculature), resemble the natural, physiological haemodynamics. Thus, the presented numerical simulations can be considered as successfully validated.

3.2. Common carotid artery bifurcation

The first analysed aspect was the flow distribution across the numerical domain. For this purpose, three control planes were created at the distal part of the common carotid artery (CCA), the internal carotid artery (ICA) and the external carotid artery (ECA) – for steady-state simulations, the area-averaged velocity was examined, while for transient ones, the blood volume delivered throughout the entire cardiac cycle was calculated (Tab. 8). Based on the presented data, it can be concluded that the influence of the blood model on the flow distribution seems to be negligible for the majority of the case studies. The highest differences were obtained for the Power Law and K-L models, at 2.8% and 1.7%, respectively. For the Carreau, Cross, Modified Power Law and Quemada models, hardly any discrepancies could be observed. Within this group, the highest deviation was circa 0.5%. Conducted steady-state and transient simulations indicate that the flow distribution within the CCA bifurcation model is not affected significantly by the rheological blood model; however, some alternations occur. This suggests that blood can be simplified to a Newtonian fluid when analysing a CCA bifurcation. To prove the aforementioned statement, an additional analysis of further haemodynamic parameters was required. Tab. 9 outlines area-averaged wall shear stress (AAWSS) and area-averaged spatial gradient of wall shear stress (AAWSSG) calculated for the model walls. Additionally, average and maximum time-averaged wall

shear stress (TAWSS) and shear index (OSI) values are shown as well.

Tab. 8. Blood distribution analysis for the CCA bifurcation geometry

	Control plane	Blood model							
		NEWT	CAR	CAS	CRO	KL	MPL	PL	QUE
Avg. velocity [m/s]	P1	**0.386**	**0.385** (–0.3%)	**0.385** (–0.3%)	**0.386** (0.0%)	**0.385** (–0.3%)	**0.386** (0.0%)	**0.386** (0.0%)	**0.386** (0.0%)
	P2	**0.779**	**0.777** (–0.3%)	**0.772** (–0.9%)	**0.779** (0.0%)	**0.767** (–1.5%)	**0.779** (0.0%)	**0.801** (2.8%)	**0.782** (0.4%)
	P3	**0.541**	**0.543** (0.4%)	**0.546** (0.9%)	**0.541** (0.0%)	**0.550** (1.7%)	**0.542** (0.2%)	**0.528** (–2.4%)	**0.539** (–0.4%)
Blood vol. [cm^3]	P1	**12.004**	**12.004** (0.0%)	**12.004** (0.0%)	**12.004** (0.0%)	**12.004** (0.0%)	**12.004** (0.0%)	**12.004** (0.0%)	**12.004** (0.0%)
	P2	**5.436**	**5.408** (–0.5%)	**5.380** (–1.0%)	**5.433** (–0.1%)	**5.345** (–1.7%)	**5.415** (–0.4%)	**5.521** (1.6%)	**5.446** (0.2%)
	P3	**6.569**	**6.597** (0.4%)	**6.626** (0.9%)	**6.572** (0.0%)	**6.660** (1.4%)	**6.590** (0.3%)	**6.485** (1.3%)	**6.560** (–0.1%)

Based on the data presented in Tab. 8, it can concluded that all the parameters related to the shear stress depend on the chosen blood model. The absolute differences of the AAWSS seem to be marginal; however, they represent a significant relative variation. Thus, if a larger inflow was assumed, the absolute differences could be higher. Nevertheless, the highest AAWSS values occurred at peak systole due to the highest shear rates. Simultaneously, the absolute differences between AAWSS were the largest among all blood models, exceeding 3.5 Pa (over 40%) for the Power Law model case study. In terms of maximum TAWSS differences, the highest ones were obtained for the Power Law model (circa 20 Pa, i.e. 47%) and for the KL model (circa 12 Pa, i.e. 28%). For steady-state and transient analyses, the Newtonian fluid model underestimated AAWSS, TAWSS and AAWSSG parameters, which is in agreement with several scientific studies [2,16].

Tab. 9. Shear-related parameters for the CCA bifurcation geometry

Parameter		Blood model							
		NEWT	CAR	CAS	CRO	KL	MPL	PL	QUE
Steady-state	AAWSS [Pa]	**6.52**	**6.71** (2.9%)	**7.35** (12.7%)	**6.52** (0.0%)	**8.12** (24.5%)	**6.48** (–0.6%)	**4.21** (–35.4%)	**6.13** (–6.0%)
	AAWSSG [Pa/m]	**0.779**	**0.777** (–0.3%)	**0.772** (–0.9%)	**0.779** (0.0%)	**0.767** (–1.5%)	**0.779** (0.0%)	**0.801** (2.8%)	**0.782** (0.4%)
Systole peak	AAWSS [Pa]	**8.92**	**9.19** (3.0%)	**10.11** (13.3%)	**8.93** (0.1%)	**11.24** (26.0%)	**8.89** (–0.3%)	**5.33** (–40.2%)	**8.32** (–6.7%)
	AAWSSG [Pa/m]	**4,156**	**4,187** (0.7%)	**4,546** (9.4%)	**4,156** (0.0%)	**4,964** (19.4%)	**4,131** (–0.6%)	**2,215** (–46.7%)	**3,847** (–7.4%)
Full cycle	Avg. TAWSS [Pa]	**3.27**	**3.42** (4.6%)	**3.73** (14.1%)	**3.27** (0.0%)	**4.13** (26.3%)	**3.30** (0.9%)	**2.31** (–29.4%)	**3.12** (–4.6%)
	Max. TAWSS [Pa]	**42.97**	**43.94** (2.3%)	**48.96** (13.9%)	**42.99** (0.0%)	**54.89** (27.7%)	**42.49** (–1.1%)	**22.72** (–47.1%)	**39.33** (–8.5%)
	Avg. OSI [-]	**0.156**	**0.151** (–3.2%)	**0.151** (–3.2%)	**0.156** (0.0%)	**0.149** (–4.5%)	**0.150** (–3.8%)	**0.154** (–1.3%)	**0.154** (–1.3%)

The next analysed parameters were those related to viscosity: local and global non-Newtonian importance factors (IL and IG, respectively), as indicated in Tab. 10 and Fig. 4. If the value of the IL parameter differs from 1.0, it is possible to observe regions of the non-Newtonian flow. However, this requires a graphical representation of the analysed case – calculating a simple average value of IL does not provide meaningful information about the global influence of the rheological model. Thus, the second parameter introduced, IG, considers a relative difference in viscosity values (for each mesh node), which is averaged. After thorough numerical analyses, Johnston et al. [4] concluded that the most optimal cut-off value of IG for coronary arteries is 0.25. Below this value, the flow can be treated as Newtonian. For large arteries, a threshold value of 0.15 has been established [16].

Tab. 10. Viscosity-related parameters for the CCA bifurcation geometry

Parameter		Blood model							
		NEWT	CAR	CAS	CRO	KL	MPL	PL	QUE
Steady-state	Avg. I_L [-]	1.00	1.16	1.31	1.04	1.53	1.18	0.73	0.99
	I_G [-]	0.00	0.15	0.21	0.14	0.35	0.32	0.32	0.09
Systole start	Avg. I_L [-]	1.00	1.31	1.39	1.07	1.58	1.43	1.11	1.11
	I_G [-]	0.00	0.25	0.27	0.16	0.39	0.44	0.25	0.13
Systole peak	Avg. I_L [-]	1.00	1.10	1.27	1.01	1.49	1.06	0.62	0.94
	I_G [-]	0.00	0.10	0.18	0.02	0.33	0.17	0.32	0.07

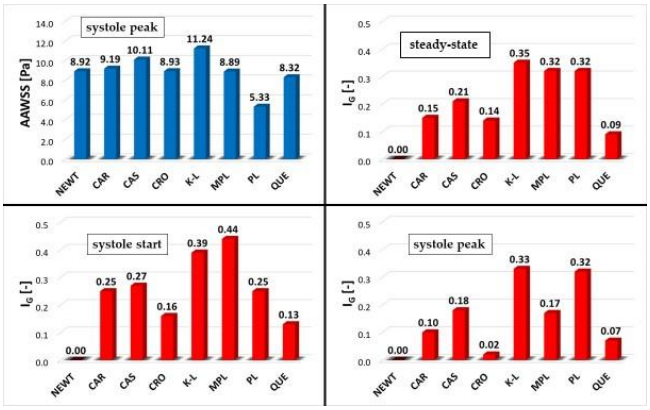

Fig. 4. AAWSS and IG parameters for the selected stages of the cardiac cycle – CCA bifurcation case studies; all rheological models of blood

Both steady-state and transient simulations outline significant deviations from the Newtonian fluid. The largest differences occur at low shear rates, i.e. at the beginning of systole. However, even at high shear rates, the results show meaningful, non-negligible discrepancies. Solely the Cross and Quemada models present proneness to Newtonian behaviour. Comparing the calculated data for steady-state analyses, the IG parameter is the highest for K-L, Modified Power Law and Power Law models (exceeding the value of 0.30), while the lowest one was obtained for the Quemada model, i.e. 0.09. The remaining blood models resulted in the IG parameter equal to approximately 0.15–0.20. Since the cut-off value of the IG parameter is claimed to be 0.15 for larger vessels,

sciendo
DOI 10.2478/ama-2024-0002

it can be concluded that all analysed blood models, except the Quemada one, show a considerable non-Newtonian character. As far as the transient simulations are concerned, similar characteristics can be observed as for the steady-state simulations, although only for the beginning of systole. This phase of the cardiac cycle is characterised by low shear rates where the blood viscosity is extremely susceptible to mathematical description. All blood models, except for Quemada, resulted in IG values greater than 0.15.

However, when systole peak occurs, meaningful changes in the IG parameter can be observed. For instance, in the Carreau and Cross models, IG drops below 0.1, whereas in the Casson and Modified Power Law models it is reduced from 0.27 and 0.44 to 0.18 and 0.17, respectively. In summary, the changes in IG resulting from varying shear rates (a consequence of varying flow velocity) indicate that the non-Newtonian behaviour of blood depends on phase of the cardiac cycle.

3.3. Entire aorta with major branches

The same results analyses were performed for the entire aorta case studies; however, to make the paper more concise, it was decided to present only the most interesting data. Thus, Tabs. 11 and 12 contain information on the selected haemodynamic parameters, i.e. blood volume delivered to specific regions of the fluid domain (P1 – gastric artery; P2 – superior mesenteric artery; P3 – left renal artery) and IL and IG parameters, as well as the maximum WSS detected at the walls. Figs. 5 and 6 depict a qualitative comparison of the selected data.

Focussing on the flow distribution, the largest difference was found at the superior mesenteric artery for the K-L blood model (6% underestimation, i.e. circa 0.35 cm3, when compared to the Newtonian reference model). For the other models, the differences varied up to 3%–4%. It can be concluded that flow distribution is not significantly affected by the mathematical description of the blood rheology, but some alternations might occur. Thus, it seems that blood can be simplified to the Newtonian fluid model when the entire aorta geometry is analysed.

Tab. 11. A quantitative analysis of the chosen parameters for the entire aorta geometry: part 1

	Control plane	Blood model							
		NEWT	CAR	CAS	CRO	KL	MPL	PL	QUE
Blood vol. [cm³]	P1	2.014	2.036 (1.1%)	2.056 (2.1%)	2.005 (–0.5%)	2.050 (1.8%)	1.998 (–0.8%)	1.997 (–0.9%)	2.023 (0.4%)
	P2	9.675	9.407 (–2.8%)	9.302 (–3.9%)	9.634 (–0.4%)	9.106 (–5.9%)	9.338 (–3.5%)	9.863 (1.9%)	9.642 (–0.3%)
	P3	6.971	6.887 (–1.2%)	6.916 (–0.8%)	6.978 (0.1%)	6.860 (–1.6%)	6.760 (–3.0%)	6.824 (–2.1%)	6.960 (–0.2%)
Steady-state; max. WSS [Pa]		11.71	12.85 (9.7%)	13.96 (19.2%)	11.94 (2.0%)	15.53 (32.6%)	12.89 (10.1%)	8.64 (–26.2%)	11.52 (–1.6%)
Systole start; max. WSS [Pa]		6.50	7.05 (8.4%)	7.84 (20.6%)	6.94 (6.8%)	8.64 (33.0%)	7.61 (17.0%)	4.98 (–23.3%)	6.56 (0.9%)
Systole peak; max. WSS [Pa]		129.53	132.35 (2.2%)	143.96 (11.1%)	130.56 (0.8%)	159.42 (23.1%)	130.38 (0.7%)	70.13 (–45.9%)	120.90 (–6.7%)
Max. TAWSS [Pa]		19.65	20.30 (3.3%)	22.22 (13.1%)	19.85 (1.0%)	24.66 (25.5%)	20.01 (1.8%)	11.19 (–43.0%)	18.40 (–6.4%)

Tab. 12. A quantitative analysis of the chosen parameters for the entire aorta geometry: part 2

Parameter	Blood model							
	NEWT	CAR	CAS	CRO	KL	MPL	PL	QUE
Systole start; I_L [-]	1.00	1.63	1.57	1.26	1.74	2.27	1.53	1.32
Systole peak; I_L [-]	1.00	1.17	1.32	1.03	1.55	1.11	0.79	1.00
Steady-state; I_G [-]	0.00	1.20	7.90	1.46	1.93	3.34	0.46	0.31
Systole start; I_G [-]	0.00	0.23	0.13	0.18	0.20	0.97	0.18	0.08
Systole peak; I_G [-]	0.00	0.02	0.04	0.00	0.10	0.03	0.04	0.00

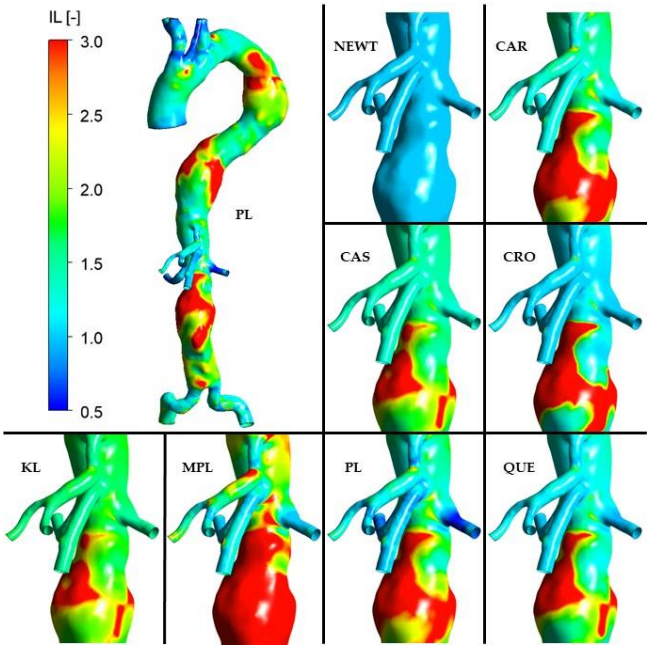

Fig. 5. Distribution of the IL parameter at the walls of the entire aorta case studies; all rheological models of blood

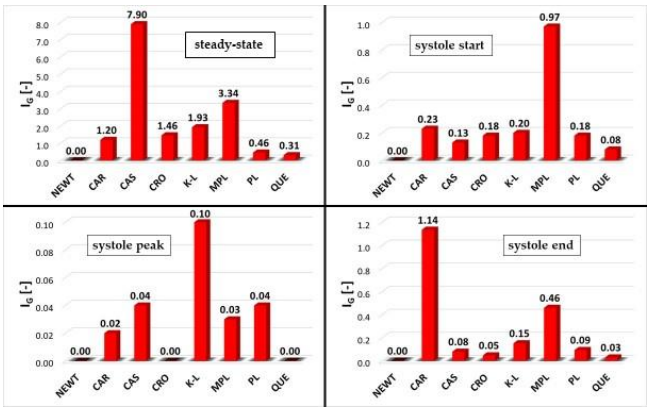

Fig. 6. The IG parameter for the selected stages of the cardiac cycle – entire aorta case studies; all rheological models of blood

A qualitative comparison of the WSS distribution also showed no significant changes between the blood models as well. However, when focussing on a quantitative comparison of WSS magnitudes as well as on IL and IG analysis, contrary observations

could be made. As shown in Tab. 11, the relative variation of the maximum WSS and TAWSS parameters was extremely high. The highest difference, obtained for the Power Law model at systole peak, was approximately 46%. The majority of the remaining differences, both for area-averaged and maximum WSS, were in the 5%–20% range. Therefore, it can be concluded that the rheological model of blood has a significant, non-negligible influence on haemodynamic parameters. This statement was further confirmed by IL and IG analysis. Concentrating on the former parameter, it can be concluded that not only the magnitudes varied, but also the general distribution was influenced by the chosen rheological model. Thus, the dynamic viscosity of the blood located in a direct vicinity of the arterial walls varied considerably in all case studies. As far as the IG parameter is concerned, a significant influence of the cardiac cycle phase on its values could be observed. At the beginning of systole, when shear rates were relatively low, almost all blood models produced IG values above the 0.15 threshold. The Casson and Quemada models were the only exceptions – the IG parameter was equal to 0.13 and 0.08, respectively. The highest value was obtained for the Modified Power Law model – it almost reached 1.00. Thus, this mathematical description is the most prone to the non-Newtonian character at the beginning of systole. At systole peak, none of the blood models reached a threshold value. Therefore, it could be concluded that at systole peak, i.e. at high shear rates, all mathematical descriptions show a high susceptibility to the Newtonian behaviour. During end-systole, the highest IG values were obtained for the Carreau and Modified Power Law models, amounting to 1.14 and 0.46, respectively. The IG parameters for the remaining blood models were characterised by values lower than 0.15.

3.4. Intracranial arterial system

During the blood distribution analysis, all outlet cross-sections were categorised into separate groups supplying different regions of the brain, i.e. anterior and middle parts of the left/right lobe and the posterior part of the left/right lobe. Tab. 13 shows the data obtained from the transient simulations, i.e. the blood volume delivered throughout the full cardiac cycle. As can be seen, the flow distribution remained almost unchanged – all differences did not exceed 1%. The largest discrepancies occurred in the K-L model, where the blood supply in the posterior part of the left lobe was limited by 0.8%. However, such small differences prove that flow distribution does not depend on the chosen blood model. It means that blood can be simplified to the Newtonian fluid model when analysing intracranial vessels. An additional analysis of parameters related to shear stresses was performed to prove this statement (Tab. 14).

Similar to the CCA bifurcation analysis, it can be seen that the absolute differences of the AAWSS, AAWSSG and TAWSS parameters are negligible, although their percentage variations are high. The Power Law and Quemada models seem to underestimate all the parameters related to the shear stress, i.e. AAWSS, AAWSSG, TAWSS and OSI. The flow solution obtained for the Cross model showed that this mathematical description is by far the most similar to the Newtonian behaviour – the results were extremely similar to the those obtained for the reference case study. Excluding the K-L and Quemada models, the remaining ones appear to result in negligible absolute differences in AAWSS, AAWSSG and TAWSS. Additionally, the general distribution of the shear-related parameters was almost identical in each case study, making a sole qualitative comparison insufficient. Fig. 7 shows a WSS comparison for two models that were characterised by the highest visual discrepancies.

Tab. 13. A quantitative analysis of the blood distribution in the cerebral vasculature case studies

	Blood volume delivered during full cardiac cycle [cm³]							
	NEWT	CAR	CAS	CRO	KL	MPL	PL	QUE
Left lobe; anterior and middle	3.445	3.438 (–0.2%)	3.437 (–0.2%)	3.445 (0.0%)	3.434 (–0.3%)	3.433 (–0.3%)	3.430 (–0.4%)	3.441 (–0.1%)
Left lobe; posterior	1.424	1.421 (–0.2%)	1.417 (–0.5%)	1.424 (0.0%)	1.411 (–0.8%)	1.426 (0.1%)	1.427 (0.2%)	1.426 (0.1%)
Right lobe; anterior and middle	3.304	3.314 (0.3%)	3.311 (0.2%)	3.306 (0.1%)	3.310 (0.2%)	3.318 (0.4%)	3.319 (0.5%)	3.311 (0.2%)
Right lobe; posterior	1.547	1.551 (0.3%)	1.553 (0.4%)	1.548 (0.1%)	1.557 (0.6%)	1.547 (0.0%)	1.547 (0.0%)	1.548 (0.1%)

Tab. 14. A quantitative analysis of shear-related parameters in the cerebral vasculature case studies

Parameter		Blood model							
		NEWT	CAR	CAS	CRO	KL	MPL	PL	QUE
Steady-state	AAWSS [Pa]	2.94	3.13 (6.5%)	3.44 (17.0%)	2.95 (0.3%)	3.85 (31.0%)	2.94 (0.0%)	2.22 (–24.5%)	2.83 (–3.7%)
	AAWSSG [Pa/m]	1,776	1,791 (0.9%)	1,934 (8.9%)	1,774 (–0.1%)	2,099 (18.2%)	1,743 (–1.8%)	1,200 (–32.4%)	1,670 (–6.0%)
Systole peak	AAWSS [Pa]	4.82	5.12 (6.2%)	5.65 (17.2%)	4.83 (0.2%)	6.38 (32.4%)	4.79 (–0.6%)	3.34 (–30.7%)	4.57 (–5.2%)
	AAWSSG [Pa/m]	3,004	3,051 (1.6%)	3,297 (9.8%)	3,002 (–0.1%)	3,600 (19.8%)	2,972 (–1.1%)	1,868 (–37.8%)	2,808 (–6.5%)
Full cycle	Avg. TAWSS [Pa]	2.29	2.47 (7.9%)	2.71 (18.3%)	2.30 (0.4%)	3.03 (32.3%)	2.32 (1.3%)	1.79 (–21.8%)	2.22 (–3.1%)
	Avg. OSI [-]	0.204	0.204 (0.0%)	0.204 (0.0%)	0.204 (0.0%)	0.204 (0.0%)	0.204 (0.0%)	0.203 (–0.5%)	0.204 (0.0%)

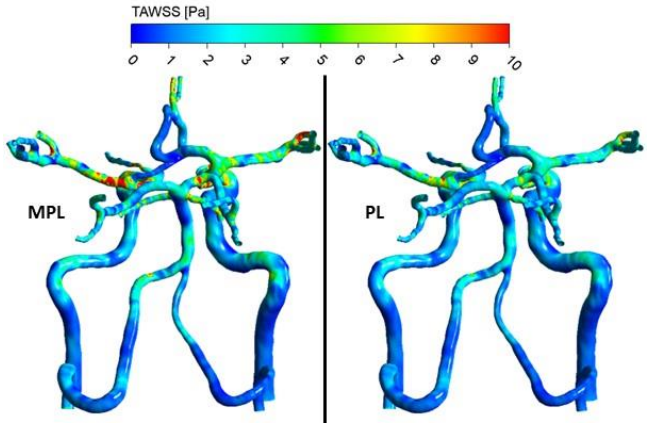

Fig. 7. TAWSS distribution at the walls of intracranial arteries – comparison of two selected rheological models: Modified Power Law (MPL) and Power Law (PL)

Therefore, the conducted analyses indicate that blood can be simplified to the Newtonian fluid model in numerical simulations of blood flow within the intracranial arteries. This was further supported by a thorough analysis of the IG parameter (see Fig. 8).

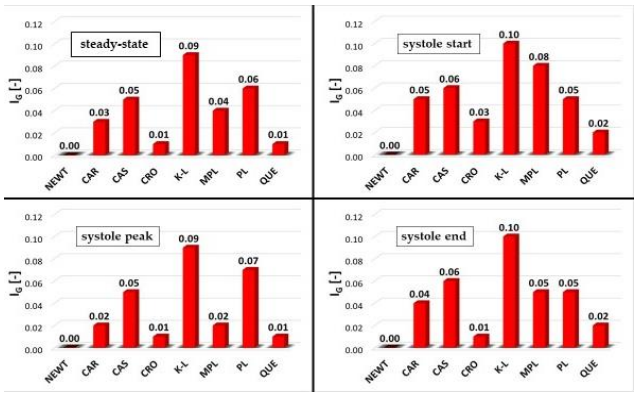

Fig. 8. The IG parameter for the selected stages of the cardiac cycle – cerebral vasculature case studies; all rheological models of blood

Contrary to the analysis performed for the CCA bifurcation and entire aorta case studies, the IG parameter for the intracranial arteries seemed to be independent of shear rate – it remained identical at both low and high shear rates. The only exception was MPL – it decreased from 0.08 (for the beginning of systole) to 0.02 (for the systole peak). The highest value of IG was obtained for the K-L model, which means that this mathematical description showed the highest non-Newtonian proneness among all investigated blood models. Moreover, regardless of the rheological model of blood, simulation type and cardiac cycle stage, all IG values were far below the threshold value of 0.15. Therefore, it can be concluded that the Newtonian model assumption of blood is a sufficient and valid approach to simulate blood flows within cerebral vasculature models.

3.5. Blood washout analysis

The final part of this research was devoted to an investigation of whether blood rheology affects the blood washout. If the remaining volume of "old blood" changed due to a mathematical description of fluid rheology, then it could be concluded that blood has to be modelled as non-Newtonian fluid in every CFD analysis. The reason behind this statement is the fact that non-washed-out blood is related to stagnation zones in which blood could start clotting. Tab. 15 presents the ratio of "old blood" that remained in the fluid domain at the last timestep of each simulation and Tab. 16 shows absolute differences of "old blood" volume, whereas Fig. 9 depicts time-dependent trends for Newtonian fluid – waveforms just for a single blood model are depicted for a clearer representation.

Firstly, it can be easily observed that the larger the model, the longer the blood washout phenomenon – for the CCA bifurcation almost the entire volume of "old blood" (~98%) was washed out during the first two cycles, whereas for the aorta case studies it took 10 cycles to reach nearly 95% of "old blood" washout. Regarding the differences in "old blood" volume remaining in the numerical domain at the end of each simulation, the relative differences seemed to be marginal – the highest discrepancy was found for the aorta geometry for the KL blood model: approximately 0.7%. Thus, such small differences suggest that blood rheology has almost no influence on the blood washout phenomenon. However, when comparing the absolute differences, slightly contrary conclusions could be drawn. For the CCA bifurcation and intracranial arteries, these differences were negligible (far below 0.01 cm3), whereas for the aorta case studies they were significant, i.e. reaching almost 4 cm3. This difference in blood volume indicated regions that could be prone to blood stagnation and, consequently, blood clotting. By applying a simple Newtonian fluid, such an observation could not be deduced.

Tab. 15. The percentage ratio of "old blood" volume with respect to the entire fluid domain volume at the end of each simulation

	Ratio of "old blood" that remained in the fluid domain [%]							
	NEWT	CAR	CAS	CRO	KL	MPL	PL	QUE
CCA bifurcation	0.37	0.41	0.41	0.39	0.42	0.40	0.31	0.39
Entire aorta	5.03	5.36	5.66	5.09	5.74	5.46	4.52	4.94
Intracranial arteries	0.60	0.62	0.62	0.64	0.64	0.67	0.52	0.61

Tab. 16. The absolute differences of "old blood" volume with respect to the volume estimated for Newtonian blood model

	Difference of "old blood" volume [cm^3]							
	NEWT	CAR	CAS	CRO	KL	MPL	PL	QUE
CCA bifurcation	-	0.002	0.002	0.001	0.002	0.001	–0.002	0.001
Entire aorta	-	1.759	3.359	0.320	3.785	2.293	–2.719	–0.480
Intracranial arteries	-	0.002	0.002	0.004	0.004	0.007	–0.008	0.001

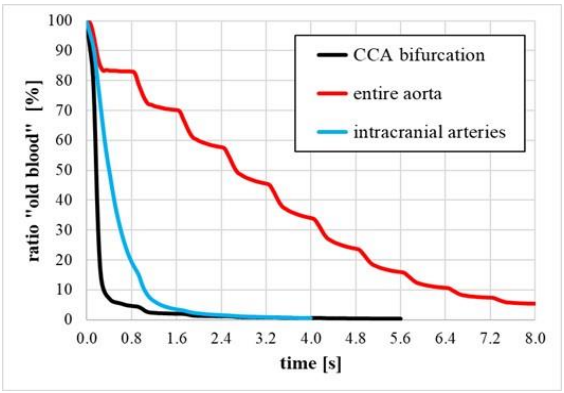

Fig. 9. The ratio of non-washed-out blood vs time – the Newtonian blood model case studies

3.6. Shear rate analysis

To observe the local influence of the rheological model of blood on the numerical data related to the flow characteristics, it was decided to perform an investigation of the shear rate at numerous control planes. Such an approach was presented in the work of Apostolidis et al. [34], who performed transient simulations of the blood flow in the left coronary artery and analysed the differences between the results obtained for the Newtonian and Casson viscoelastic models of blood. Additionally, they proposed a new approach towards setting outlet boundary conditions that attempts to preserve consistency with the pressure/flow predictions while being more computationally efficient.

To maintain the clarity of this paper, the results are presented for only one control plane per each case study. For the CCA bifurcation case study, a distal fragment of the ICA was chosen.

DOI 10.2478/ama-2024-0002

For the entire aorta case study, we decided to focus on the superior mesenteric artery (SMA), whereas in the cerebral vasculature, a cross-section of the left middle cerebral artery (MCA) was selected. Figs. 10, 11 and 12 outline a qualitative comparison of the shear rate for three selected rheological models of blood, i.e. Newtonian, Casson and Modified Power Law. The results were extracted from the time step corresponding to the late diastole, when velocity and shear rate were the lowest, whereas the non-Newtonian proneness was the highest. Apart from a qualitative comparison of shear rate, we decided to present a relative difference (expressed as a percentage) between non-Newtonian and Newtonian models. All differences below 10% were considered insignificant. Therefore, a dark blue colour represents regions where the shear rate differences were negligible. The quantitative data of this analysis are presented in Tab. 17.

Tab. 17. Analysis of relative differences in shear rate

Control surface	Max. difference		Avg. difference	
	NEWT vs CAS	NEWT vs MPL	NEWT vs CAS	NEWT vs MPL
ICA	114.0%	30.9%	12.6%	5.2%
SMA	116.8%	113.3%	24.0%	34.4%
MCA	86.5%	17.8%	8.5%	1.6%

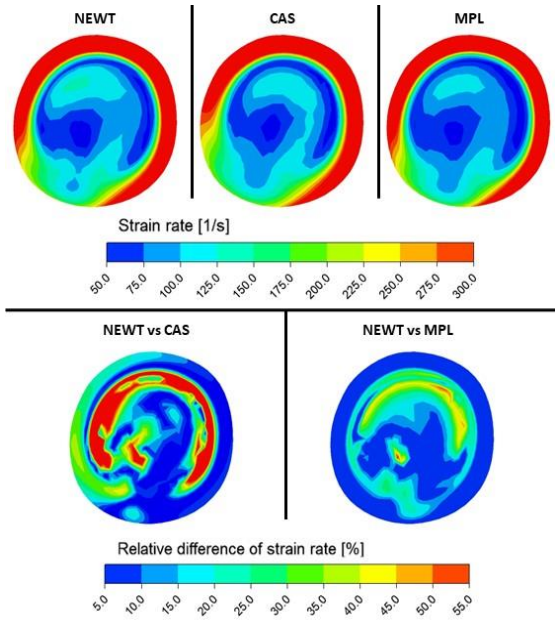

Fig. 10. The shear rate distribution and its relative differences at the ICA plane for three rheological models of blood – the CCA bifurcation case

By analysing the quantitative and qualitative data presented in Tab. 17 and Figs. 10, 11 and 12, it can be concluded that the rheological model of blood influenced the shear rate in each case study. Focussing on the maximum differences, the highest discrepancies were found for the superior mesenteric artery (SMA), exceeding 115%. Regarding the average differences, the highest ones were once again found at the SMA control surface (24.0% and 34.4% for Casson and Modified Power Law models, respectively). The lowest discrepancies were observed at MCA surface for Modified Power Law model – i.e. 1.6%. It is interesting to note that the differences in shear rate for the MPL model were visible only in the free-flow regime and not in the boundary layer. For the other control surfaces and rheological models, differences could be observed both in the free-flow regime and in the boundary layer. Additionally, the discrepancies were significant, confirming all the former conclusions that blood should not be modelled as a simple Newtonian fluid.

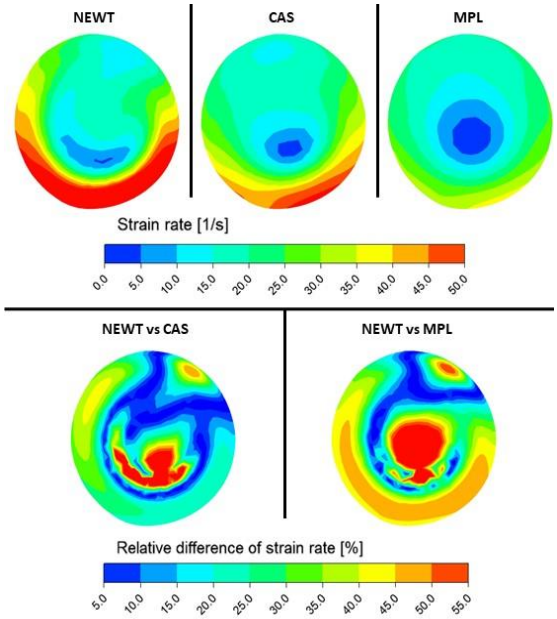

Fig. 11. The shear rate distribution and its relative differences at the SMA for three rheological models of blood – the entire aorta case

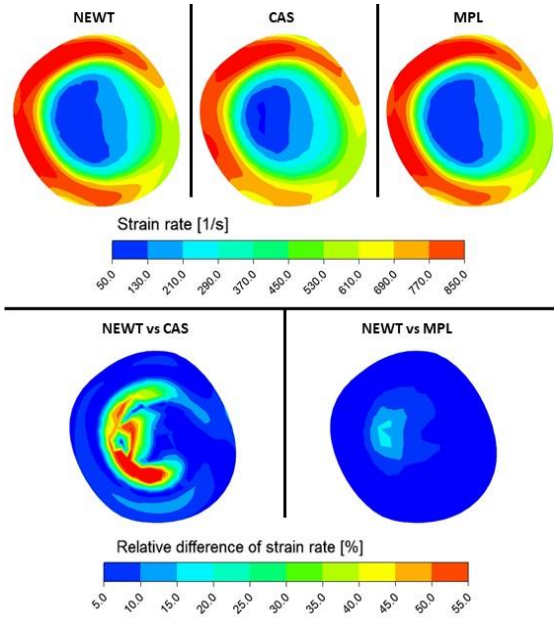

Fig. 12. The shear rate distribution and its relative differences at the left MCA for three rheological models of blood – the cerebral vasculature study

4. DISCUSSION

The vast majority of studies available in the literature present the results of blood flow simulations in a specific fragment of the arterial system. We, on the other hand, decided to carry out a research (dedicated to numerical analyses of blood flows characterised by different rheological models of blood) using three ge-

ometries of varying complexity and location in the circulatory system. This allowed us to consider a possible influence of the arterial system complexity on the numerical data. Moreover, to generate as much data as possible, we decided to analyse a large number of different haemodynamic parameters and other possible bioindicators to ensure that the conclusions we drew were correct and adequately supported. It should be emphasised that we coupled rheology analyses with simulating the blood washout phenomenon. Unfortunately, there are no other literature data with which we could compare such results – this indicates an innovative approach towards rheology investigations. Furthermore, one of the analysed parameters was the shear rate. This investigation showed that the viscosity models have a significant effect on the shear rate, especially for the common carotid artery and the entire aorta case studies. Similar observations, i.e. non-negligible differences between Casson and Newtonian models, were presented in the work of Apostolidis et al. [34]. However, they simulated blood flow in the other blood vessel, i.e. the coronary artery, and thus a direct comparison between the two data sets could not be made.

Conducted steady-state and transient simulations indicate that the flow distribution within the CCA bifurcation model was not significantly affected by the rheological blood model; however, some changes occurred. Similarly, Mendieta et al. [13] did not observe drastic changes – flow rate and flow patterns were similar between case studies. This is in contrast to the work of Gijsen et al. [10], who claimed that there is a considerable difference in velocity distribution between the Newtonian and Carreau–Yasuda models. According to their research, the non-Newtonian fluid was characterised by a flattened axial velocity profile and lower velocity gradients. However, no quantitative comparison was presented, and thus it is not clear whether the differences exceed 2%, 5% or 10%. Moreover, we did not see any significant differences in the "old blood" volume remaining in the numerical domain at the end of the simulation. The largest deviation was far below 0.01 cm3. This suggests that rheology does not play a critical role in simulating blood flows in CCA models. Although the flow distribution was almost unaffected by the blood rheology (except for the Power Law model), we noticed a significant difference in the shear rate during the quantitative and qualitative evaluation. Additionally, high values of IG and IL parameters suggested that the blood model affected the flow haemodynamics. This statement and most of the presented results are in agreement with the findings of Shinde et al. [11], Razavi et al. [14], Gharahi et al. [35] and Moradicheghamahi et al. [36]. The Newtonian fluid model underestimated AAWSS, TAWSS and AAWSSG parameters, which is consistent with the research of Caballero and Lain [2]. The K-L model overestimated the aforementioned parameters, while the Cross model seemed to be the most prone to Newtonian behaviour – results were almost identical to those obtained for the Newtonian fluid. Similar to the work of Moradicheghamahi et al. [36], the AAWSS values were the smallest for Newtonian fluid among all models (Power Law is an exception), while the OSI was the largest.

As far as entire aorta case studies are concerned, the flow distribution was not significantly affected by the blood rheology; however, some changes could be observed. Thus, it appears that blood can be simplified to the Newtonian fluid model when the entire aorta geometry is analysed. The research of Karimi et al. [16] suggests that the Cross model generates considerably different velocity distributions at lower shear rates (during diastole), which is opposed to the results of the performed simulations. Despite negligible differences in flow distribution, blood washout analysis showed significant discrepancies between rheological models of blood, reaching nearly 4 cm3 for the K-L model. By simplifying blood to a Newtonian fluid, it would not be possible to detect regions characterised by blood stagnation and blood clotting. Moreover, it turned out that we obtained non-negligible differences in the magnitude of the shear rate at several control planes. The largest discrepancy exceeded 115% for the Casson model at the superior mesenteric artery. A thorough analysis of the IG parameter showed that the intensity of the rheological model influence varied, depending on the cardiac cycle phase. At the beginning of systole, almost all blood models produced IG values above 0.15, i.e. above the threshold value presented by Karimi et al. [16]. Therefore, treating blood as a simple Newtonian fluid might be an oversimplification. When comparing the absolute differences among area-averaged WSS and TAWSS, they appeared to be marginal. This may indicate that the blood rheology influence is negligible in the aorta model, which is in agreement with the research of Caballero et al. [2]. Additionally, after qualitative analysis of WSS and TAWSS distributions, these authors concluded that the assumption of the non-Newtonian fluid is not necessary under pulsatile flow, since hardly any differences were visible in the figures. Such conclusions are consistent with the results of this research. However, when the maximum WSS values were analysed quantitatively, no higher absolute differences could be observed, reaching even 60 Pa. Therefore, despite small absolute differences of AAWSS and similar WSS distributions at the model wall, high differences in the maximum WSS and high percentage variation of all parameters suggest that blood should be modelled as a shear-thinning fluid for the aorta.

In terms of intracranial arteries, the flow distribution remained nearly unchanged – all differences did not exceed 1%. Thus, it was demonstrated that the flow distribution does not depend on the chosen blood model. Additionally, hardly any differences could be detected in blood washout analysis, suggesting that blood can be treated as a Newtonian fluid when intracranial vessels are analysed. Such a result is in agreement with the work of Razavi et al. [37], who claimed that Newtonian fluid is a sufficient simplification of the blood model when it comes to the cerebral vasculature. Moreover, not only negligible differences in flow distribution were obtained, but also WSS, TAWSS and WSSG did not change significantly when compared to the reference case. A similar observation could be made when analysing the shear rate at the investigated cross-sections. For example, the average difference between MPL and Newtonian models was only 1.6%. Additionally, the shear rate changes could only be observed in the free-flow regime, and thus they did not influence the parameters related to the stress exerted on the arterial walls (pressure and WSS). Furthermore, the IG results were far below the thresholds suggested by two research teams, which supports the aforementioned statement [4,16]. Oliveira et al. [38] noticed a 50% overestimation of the maximum WSS values at intracranial aneurysm walls. However, when TAWSS and AAWSS were considered, the relative differences decreased to less than 7%. Nevertheless, they concluded that the non-Newtonian assumption of blood is recommended when investigating the maximal WSS and OSI at systole peak.

5. CONCLUSIONS

We present a comprehensive study in which we analysed the influence of eight different rheological models of blood on the

numerical results. To ensure that valid conclusions were drawn, we performed in-silico investigations of blood flows in geometries of varying complexity (CCA bifurcation, entire aorta and cerebral vasculature). Thus, our research was not limited to only one type of the arterial configuration. Furthermore, this study was based on the analysis of numerous haemodynamic parameters and bioindicators, including flow distribution, WSS, TAWSS, WSSG, OSI, IG, IL and shear rate. Moreover, we coupled the rheology assessment with the blood washout phenomenon.

The main conclusion of this research is that all haemodynamic parameters, and their variation resulting from different blood models, are strictly related to the model geometry and imposed boundary conditions. The results obtained during this research indicate that blood can be simplified to the Newtonian fluid model when cerebral vasculature is analysed, whereas for the CCA bifurcation and large vessels network it should be modelled as a shear-thinning fluid. Therefore, regardless of the geometry topology, boundary conditions and simulation type, it is more advisable to provide formulas that describe the non-Newtonian behaviour of blood. Otherwise, the simulation might be oversimplified while the results might be underestimated.

REFERENCES

1. Reorowicz P, Obidowski D, Klosinski P, Szubert W, Stefanczyk L, Jozwik K. Numerical simulations of the blood flow in the patient-specific arterial cerebral circle region. J Biomech. 2014;47(7): 1642–51.
2. Caballero AD, Laín S. Numerical simulation of non-Newtonian blood flow dynamics in human thoracic aorta. Comput Methods Biomech Biomed Engin. 2015;18(11):1200–16.
3. Doost SN, Zhong L, Su B, Morsi YS. The numerical analysis of non-Newtonian blood flow in human patient-specific left ventricle. Comput Methods Programs Biomed [Internet]. 2016;127:232–47. Available from: http://dx.doi.org/10.1016/j.cmpb.2015.12.020
4. Johnston BM, Johnston PR, Corney S, Kilpatrick D. Non-Newtonian blood flow in human right coronary arteries: Steady state simulations. J Biomech. 2004;37(5):709–20.
5. Jodko D, Jeckowski M, Tyfa Z. Fluid structure interaction versus rigid-wall approach in the study of the symptomatic stenosed carotid artery: Importance of wall compliance and resilience of loose connective tissue. Int j numer method biomed eng. 2022;38(8):1–23.
6. Reorowicz P, Tyfa Z, Obidowski D, Wiśniewski K, Stefańczyk L, Jóźwik K, et al. Blood flow through the fusiform aneurysm treated with the Flow Diverter stent – Numerical investigations. Biocybern Biomed Eng. 2022;42(1):375–90.
7. Tyfa Z, Obidowski D, Reorowicz P, Stefańczyk L, Fortuniak J, Jóźwik K. Numerical simulations of the pulsatile blood flow in the different types of arterial fenestrations: Comparable analysis of multiple vascular geometries. Biocybern Biomed Eng. 2018;38(2):228–42.
8. Wisniewski K, Tomasik B, Tyfa Z, Reorowicz P, Bobeff EJ. Porous Media Computational Fluid Dynamics and the Role of the First Coil in the Embolization of Ruptured Intracranial Aneurysms. J Clin Med. 2021;10(7):1348.
9. Cho YI, Kensey KR. Effects of the non-Newtonian viscosity of blood on flows in a diseased arterial vessel. Part 1: Steady flows. Biorheology. 1991;28(3–4):241–62.
10. Gijsen FJH, Van De Vosse FN, Janssen JD. The influence of the non-Newtonian properties of blood on the flow in large arteries: steady flow in a carotid bifurcation model. J Biomech. 1999; 32(7):705–13.
11. Shinde S, Mukhopadhyay S, Mukhopadhyay S. Investigation of flow in an idealized curved artery: comparative study using cfd and fsi with newtonian and non-newtonian fluids. J Mech Med Biol [Internet]. 2022;22:2250010. Available from: https://doi.org/10.1142/S0219519422500105
12. Boyd J, Buick JM. Comparison of Newtonian and non-Newtonian flows in a two-dimensional carotid artery model using the lattice Boltzmann method. Phys Med Biol. 2007;52(20):6215–28.
13. Mendieta JB, Fontanarosa D, Wang J, Paritala PK, McGahan T, Lloyd T, et al. The importance of blood rheology in patient-specific computational fluid dynamics simulation of stenotic carotid arteries. Biomech Model Mechanobiol [Internet]. 2020;19(5):1477–90. Available from: https://doi.org/10.1007/s10237-019-01282-7.
14. Razavi A, Shirani E, Sadeghi MR. Numerical simulation of blood pulsatile flow in a stenosed carotid artery using different rheological models. J Biomech [Internet]. 2011;44(11):2021–30. Available from: http://dx.doi.org/10.1016/j.jbiomech.2011.04.023
15. Johnston BM, Johnston PR, Corney S, Kilpatrick D. Non-Newtonian blood flow in human right coronary arteries: Transient simulations. J Biomech. 2006;39(6):1116–28.
16. Karimi S, Dabagh M, Vasava P, Dadvar M, Dabir B, Jalali P. Effect of rheological models on the hemodynamics within human aorta: CFD study on CT image-based geometry. J Nonnewton Fluid Mech [Internet]. 2014;207:42–52. Available from: http://dx.doi.org/10.1016/j.jnnfm.2014.03.007
17. Celik IB, Ghia U, Roache PJ, Freitas CJ, Coleman H, Raad PE. Procedure for estimation and reporting of uncertainty due to discretization in CFD applications. J Fluids Eng Trans ASME. 2008;130(7):0780011–4.
18. Obidowski D, Reorowicz P, Witkowski D, Sobczak K, Jóźwik K. Methods for determination of stagnation in pneumatic ventricular assist devices. Int J Artif Organs. 2018;41(10):653–63.
19. Rayz VL, Boussel L, Lawton MT, Acevedo-Bolton G, Ge L, Young WL, et al. Numerical modeling of the flow in intracranial aneurysms: Prediction of regions prone to thrombus formation. Ann Biomed Eng. 2008;36(11):1793–804.
20. Logerfo FW, Nowak MD, Quist WC. Structural details of boundary layer separation in a model human carotid bifurcation under steady and pulsatile flow conditions. J Vasc Surg. 1985;2(2):263–9.
21. Subramaniam T, Rasani MR. Pulsatile CFD Numerical Simulation to investigate the effect of various degree and position of stenosis on carotid artery hemodynamics. J Adv Res Appl Sci Eng Technol. 2022;26(2):29–40.
22. Nagai Y, Kemper MK, Earley CJ, Metter EJ. Blood-flow velocities and their relationships in carotid and middle cerebral arteries. Ultrasound Med Biol. 1998;24(8):1131–6.
23. Pomella N, Wilhelm EN, Kolyva C, González-Alonso J, Rakobowchuk M, Khir AW. Common Carotid Artery Diameter, Blood Flow Velocity and Wave Intensity Responses at Rest and during Exercise in Young Healthy Humans: A Reproducibility Study. Ultrasound Med Biol. 2017;43(5):943–57.
24. Soleimani E, Mokhtari-Dizaji M, Fatouraee N, Saberi H. Assessing the blood pressure waveform of the carotid artery using an ultrasound image processing method. Ultrasonography. 2017;36(2): 144–52.
25. Lantz BM, Forester JM, Link DP, Holcroft JW. Regional distribution of cardiac output: normal values in man determined by video dilution technique. Am J Roentgenol. 1981;137(5):903–7.
26. Stein PD, Sabbah HN, Anbe DT, Walburn FJ. Blood velocity in the abdominal aorta and common iliac artery of man. Biorheology. 1979;16(3):249–55.
27. Bruss ZS, Raja A. Physiology, Stroke Volume. In: StatPearls Publishing. StatPearls Publishing; 2022.
28. Czernicki Z. Fizjologia mózgowego przepływu krwi. In: Czepko R, editor. Wybrane zagadnienia diagnostyki i leczenia malformacji naczyniowych ośrodkowego układu nerwowego. Uniwersytet Jagiellonski - Wydawnictwo Uniwersytetu Jagiellonskiego; 2007. 15–20.

29. Xing CY, Tarumi T, Liu J, Zhang Y, Turner M, Riley J, et al. Distribution of cardiac output to the brain across the adult lifespan. J Cereb Blood Flow Metab. 2017;37(8):2848–56.
30. Majka J. Fizjologia krążenia mózgowego. In: Szczudlik A, Członkowa A, Kwieciński H, Słowik A, editors. Udar mózgu. 1st ed. Kraków: Wydawnictwo Uniwersytetu Jagiellońskiego; 2007;26–41.
31. Seidel E, Eicke BM, Tettenborn B, Krummenauer F. Reference values for vertebral artery flow volume by duplex sonography in young and elderly adults. Stroke. 1999;30(12):2692–6.
32. Amin-Hanjani S, Du X, Pandey DK, Thulborn KR, Charbel FT. Effect of age and vascular anatomy on blood flow in major cerebral vessels. J Cereb Blood Flow Metab. 2015;35(2):312–8.
33. Zarrinkoob L, Ambarki K, Wåhlin A, Birgander R, Eklund A, Malm J. Blood flow distribution in cerebral arteries. J Cereb Blood Flow Metab. 2015;35(December 2014):648–54.
34. Apostolidis AJ, Moyer AP, Beris AN. Non-Newtonian effects in simulations of coronary arterial blood flow. J Nonnewton Fluid Mech [Internet]. 2016;233:155–65. Available from: http://dx.doi.org/10.1016/j.jnnfm.2016.03.008
35. Gharahi H, Zambrano BA, Zhu DC, DeMarco JK, Baek S. Computational fluid dynamic simulation of human carotid artery bifurcation based on anatomy and volumetric blood flow rate measured with magnetic resonance imaging. Int J Adv Eng Sci Appl Math. 2016;8(1):46–60.
36. Moradicheghamahi J, Sadeghiseraji J, Jahangiri M. Numerical solution of the Pulsatile, non-Newtonian and turbulent blood flow in a patient specific elastic carotid artery. Int J Mech Sci [Internet]. 2019;150(October 2017):393–403. Available from: https://doi.org/10.1016/j.ijmecsci.2018.10.046
37. Razavi SE, Farhangmehr V, Zendeali N. Numerical investigation of the blood flow through the middle cerebral artery. BioImpacts [Internet]. 2018;8(3):195–200. Available from: https://doi.org/10.15171/bi.2018.22
38. Oliveira IL, Santos GB, Gasche JL, Militzer J, Baccin CE. Non-Newtonian Blood Modeling in Intracranial Aneurysm Hemodynamics: Impact on the Wall Shear Stress and Oscillatory Shear Index Metrics for Ruptured and Unruptured Cases. J Biomech Eng [Internet]. 2021;143(7):071006. Available from: https://doi.org/10.1115/1.4050539

This work has been accomplished under the part of the research project No. LIDER/12/0056/L-10/18/NCBR/2019 financed by Polish National Centre for Research and Development.

Zbigniew Tyfa: https://orcid.org/0000-0001-9870-8370
Reorowicz Piotr: https://orcid.org/0000-0003-0585-0488
Obidowski Damian: https://orcid.org/0000-0002-8950-6424
Jóźwik Krzysztof: https://orcid.org/0000-0002-7596-3691